Release of internal molecular torque results in twists of Glaucocystis cellulose nanofibers

Yu Ogawa

▶ **To cite this version:**

Yu Ogawa. Release of internal molecular torque results in twists of Glaucocystis cellulose nanofibers. Carbohydrate Polymers, 2021, 251, pp.117102. 10.1016/j.carbpol.2020.117102 . hal-02977831

HAL Id: hal-02977831
https://hal.science/hal-02977831

Submitted on 14 Nov 2020

HAL is a multi-disciplinary open access archive for the deposit and dissemination of scientific research documents, whether they are published or not. The documents may come from teaching and research institutions in France or abroad, or from public or private research centers.

L'archive ouverte pluridisciplinaire **HAL**, est destinée au dépôt et à la diffusion de documents scientifiques de niveau recherche, publiés ou non, émanant des établissements d'enseignement et de recherche français ou étrangers, des laboratoires publics ou privés.

Release of internal molecular torque results in twists of *Glaucocystis* cellulose nanofibers

Yu Ogawa

Univ. Grenoble Alpes. CNRS, CERMAV, 38000 Grenoble, France

Email address: yu.ogawa@cermav.cnrs.fr

Phone: +33 4 76 03 76 19; Fax: +33 4 76 54 72 03

ORCid: 0000-0003-0677-7913

Abstract

The cellulose of the green alga *Glaucocystis* consists of almost pure Iα crystalline phase where the corresponding lattice b* axis parameter lies perpendicular to the cell wall surface in the multilamellar cell wall architecture, indicating that in this wall, cellulose is devoid of longitudinal twist. In contrast, when isolated from *Glaucosytis* cell walls, the cellulose microfibrils present a twisting behavior, which was investigated using electron microscopy techniques. Sequential electron microdiffraction analyses obtained under frozen hydrated conditions revealed that the cellulose microfibrils continuously right-hand twisted in the vitreous ice layer. This observation implies that the twists of these nanofibers are intrinsic to the cellulose molecule and not a result of the cell wall biogenesis process. Furthermore, scaling with the fourth power of width based on the classic mechanics of solid, the twist angle was in agreement with the reported values in higher plant celluloses, implying that the twist arises from the balance between tendency of individual chains to twist and the structure imposed by the crystal packing. The observed twist in isolated fibrils of *Glaucocystis* indicates that one cannot assume the presence of cellulose twisting *in vivo* based on observations of isolated cellulose nanoparticles, as microfibril can exist untwisted in the original cell wall but become twisted when released from the wall.

Keywords; Cellulose Iα; Cryogenic transmission electron microscopy; Electron diffraction; Twist; Nanofiber

1. Introduction

The morphology of cellulose nanoparticles, cellulose nanocrystals (CNC) and cellulose nanofibers (CNF) have extensively been studied using various scattering and microscopy techniques since this morphology strongly affects the final properties of materials involving these nanoparticles (Elazzouzi-Hafraoui et al., 2008; Foster et al., 2018; Jakob, Fratzl, & Tschegg, 1994; Mao et al., 2017). Alongside with the particle dimensions, fibrillar twists of cellulose nanoparticles are among well studied morphological features of cellulose at the nanometric scale (Hanley, Revol, Godbout, Gray, 1997; Usov et al., 2015; Nakai et al., 2013; Hirai, Tsuji, & Horii, 1998). This is because the fibrillar twists are considered to reflect the intrinsic chirality of cellulose and have high potential in high value-added applications such as a nanosized chiral inducer (Kaushik et al., 2015; Majoinen et al., 2016). While the uniaxial right-handed twists along the fiber axis of cellulose crystal have long been observed under both electron and scanning probe microscopes, the quantitative analyses of this feature have only recently been reported thanks to the methodological developments in the microscopy techniques (Arcari et al., 2019; Bai et al., 2020; Ogawa. 2019). Computational approaches such as force field simulations and quantum chemical calculations have also contributed to understanding the nanoscale geometry of the twisting of cellulose crystals (Conley, Godbout, Whitehead, & van de Ven, 2016; Dumitrică, 2020; Matthews et al., 2006; Zhao et al., 2013).

Despite the efforts for characterizing the fibrillar twists of cellulose, many questions about this twisting remain to be answered. The occurrence of the twists *in vivo* is such a question. Some authors have speculated on the presence of the cellulose twisting in higher plant cell walls (Fernandes et al., 2011; Park et al., 2013), but solid evidence is still lacking for the twisting *in planta*. In contrast, it has been well demonstrated that such a fibrillar twist does not exist in the cell walls of a series of green algae such as *Valonia*, *Oocystis*,

Micrasterias and *Glaucocystis* (Imai, Sugiyama, Itoh, & Horii, 1999; `Kim, Herth, Vuong, & Chanzy, 1996; Sugiyama, Chanzy, & Revol, 1994). In the cell wall of these green algae, the cellulose microfibrils are organized into plywood-like multilamellar structures. Each lamella consists of a parallel array of microfibrils and their orientation alternate between adjacent lamellae (Itoh & Brown, 1984; Willison & Brown, 1978). Detailed X-ray and electron diffraction studies revealed that the cellulose crystals show strict uniplanar orientations, where either *a** or *b** reciprocal axis of the triclinic Iα unit cell is always perpendicular to the lamellar plane (Imai, Sugiyama, Itoh, & Horii, 1999; Sugiyama, Chanzy, & Revol, 1994). Such a preferential orientation in the lateral plane of the crystals excludes the twisting of cellulose crystals in these algal cell wall architectures. It is unclear, however, if the absence of twist *in vivo* directly implies its absence in the isolated nanoparticle state.

In the present study, the nanoscale morphology of CNFs obtained from *Glaucocystis* was investigated using a sequential electron microdiffraction method. The method was developed in the previous report to investigate the twist geometry of tunicate CNCs that are composed of pure cellulose Iβ allomorph. In *Glaucocystis*, the cellulose microfibrils are composed almost solely of the Iα allomorph and not twisted in the cell wall (Imai, Sugiyama, Itoh, & Horii, 1999; Nishiyama, Sugiyama, Chanzy, & Langan, 2003). Thus, it is an ideal model specimen to investigate, on one hand, the effect of the isolation process and on the other hand, the effect of the allomorphic structures on the nanoscale twist geometries. Based on local crystallographic information obtained using the electron diffraction experiments, the occurrence of fibrillar twist was observed, implying that the isolation process of cellulose greatly altered the nanoscale geometry of cellulose crystals.

2. Materials and methods

2.1. Sample preparation

Cellulose microfibril suspensions from *Glaucocystis nostochinearum* were prepared using sulfamic acid according to the method previously described by Briois et al (2013). First, ghost cells of *G. nostochinearum* were prepared according to the method described by Imai et al. (1999). These ghost cells were then dispersed into dimethylformamide (DMF) by solvent exchange. The cells were transferred to 2 wt% sulfamic acid DMF solution and kept overnight at 80 °C under mild agitation. The cells were then washed three times by centrifugations in DMF and finally into the water where they spontaneously disrupted into non-flocculating suspensions of individual cellulose microfibrils. The isolated cellulose microfibrils will hereafter be referred to as CNFs.

2.2 Transmission electron microscopy (TEM)

All transmission electron microscopy was performed using a JEM-2100Plus (Jeol Ltd, Japan). All the electron micrographs and diffraction patters were recorded using a Gatan Rio 16 camera (Gatan Inc., USA) using the SerialEM program (Mastronarde, 2003). The sample preparation and observation procedures for both conventional and cryogenic conditions were described in a previous report (Ogawa, 2019).

3. Results

3.1. Morphology of *Glaucocystis* CNFs.

Figure 1 shows cryogenic (Fig. 1a) and negatively stained (Figs. 1b and 1c) TEM images of *Glaucocystis* CNFs. Individual CNFs were well dispersed and isolated after the sulfamic acid treatment as reported previously (Briois et al., 2013). The sulfamic acid treatment was chosen in this study as it provided long and straight nanofibers compared to the short ones resulting from strong acid hydrolysis treatments, due to the less destructive nature of the sulfamic treatment. As seen in Fig. 1c, the *Glaucocystis* CNFs show a wide distribution

104 of fibril width. The average width was estimated as 8.8 ± 3.0 nm from the negatively stained
105 images. There are slight changes in width along the fiber direction as indicated by
106 arrowheads in Figs. 1b and 1c, likely indicative of the presence of the fibrillar twist. While
107 they are more noticeable in the negatively stained images than in the cryoTEM counterparts,
108 this apparent width distribution is much less important compared to those in cellulose
109 microfibrils from other sources such as tunicate and bacteria (Elazzouzi-Hafraoui et al., 2008;
110 Usov et al., 2015). This is not surprising considering the difference in the cross-sectional
111 shapes of these cellulose microfibrils. The *Glaucocystis* microfibril has an approximately
112 square cross section while those of tunicate and bacterial cellulose microfibrils are more
113 elongated on one side of cross-sections than the other (Imai et al., 1999; Helbert, Nishiyama,
114 Okano, & Sugiyama 1998; Fang & Catchmark, 2014). As illustrated in Fig. 1d, a fiber with a
115 square cross section shows a smaller width modification along a 180° fibrillar twist compared
116 to ones presenting more elongated rectangular cross sections. This feature indicates a
117 potential drawback of conventional imaging and highlights the importance of using
118 crystallographic information to decipher the detailed twist geometry of cellulose crystals.
119

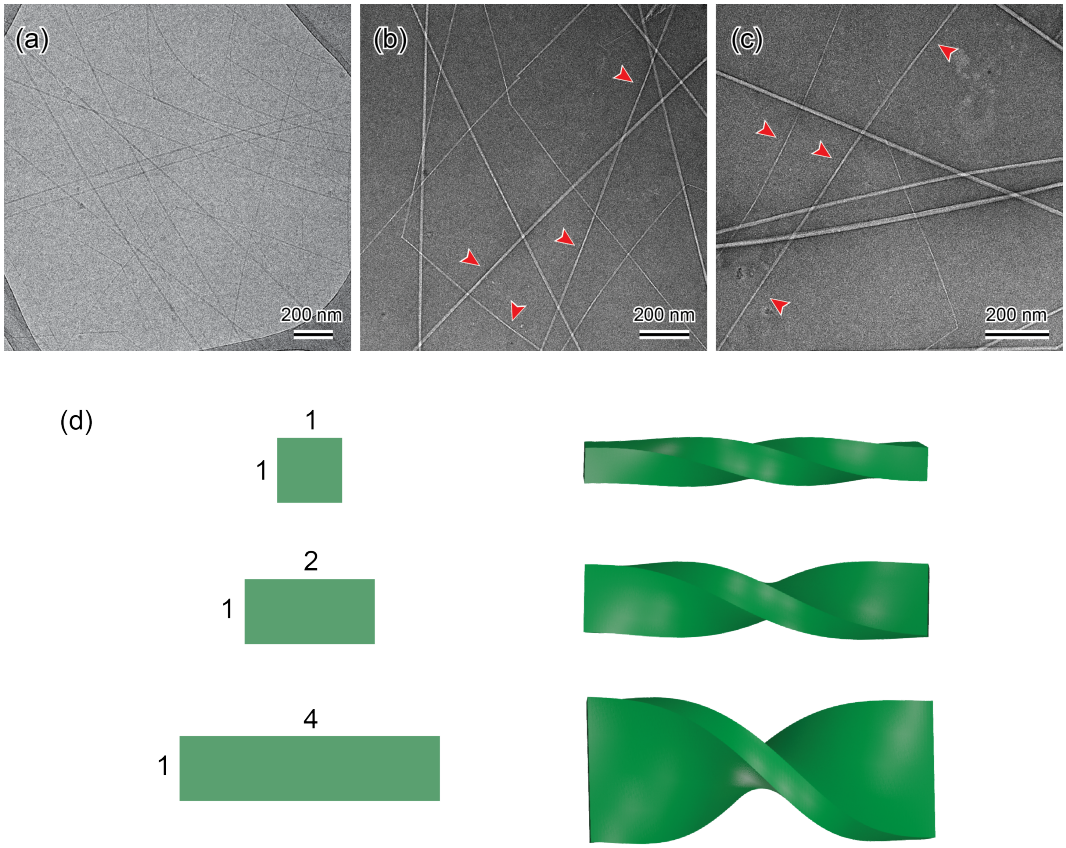

120

121 **Figure 1.** Morphology of *Glaucocystis* CNFs. (a) Diffraction contrast image of *Glaucocystis*
122 CNFs in vitreous ice layer. (b, c) Negatively stained images of *Glaucocystis* CNFs dried on
123 an amorphous carbon film. Arrowheads indicate apparent twist regions. (d) Schematic
124 illustrations of width modification of twisted fibrils (right) with different cross-sectional
125 shapes (left).

126

127 **3.2. Twist geometry of *Glaucocystis* CNFs followed by electron microdiffraction**

128 The twist geometry of *Glaucocystis* CNFs was then investigated using the electron
129 microdiffraction technique using the method previously described (Ogawa, 2019). The
130 electron microdiffraction allows obtaining local crystallographic information at a single
131 nanoparticle level. Since the crystal structure of cellulose Iα and the cross-sectional shape
132 have been established in the literature (Imai et al., 1999; Nishiyama, Sugiyama, Chanzy, &
133 Langan, 2003), one can determine the twist geometry of a CNF based on crystallographic

orientation obtained from two-dimensional microdiffraction data and the reported information of the *Glaucocystis* cellulose crystal.

Figure 2 summarizes the microdiffraction analysis of a *Glaucocystis* CNF in vitreous ice layer. The studied CNF is slightly curved as described in the literature (Imai et al., 1999). There is no visible kink or defect in the studied area. The diffraction patterns were taken with an interval of 2-300 nm and over a length of ca. 5.5 μm along the single CNF. As shown in Fig. 2b, the diffraction patterns correspond to various projections depending on positions along the CNF, indicating that it is rotated along its fiber axis. The patterns are successively changing without showing identical diffraction patterns in consecutive positions. This implies that the *Glaucocystis* CNF is continuously twisted in the vitreous ice layer and therefore in the aqueous suspension. The twist rates of different areas along the single CNF are not constant: 6.75°/100 nm between the positions 1 to 6, 8.2°/ 100 nm between 6 to 11, 8.4° / 100 nm between 11 to 16, and 12°/ 100 nm between 16 to 19. The occurrence of the continuous twisting in the aqueous suspension was also observed for the tunicate CNCs, and the reported twist rates of the tunicate CNCs in the vitreous ice, 5-13°/ 100 nm, are comparable to those of the *Glaucocystis* CNF in the present study (Ogawa, 2019).

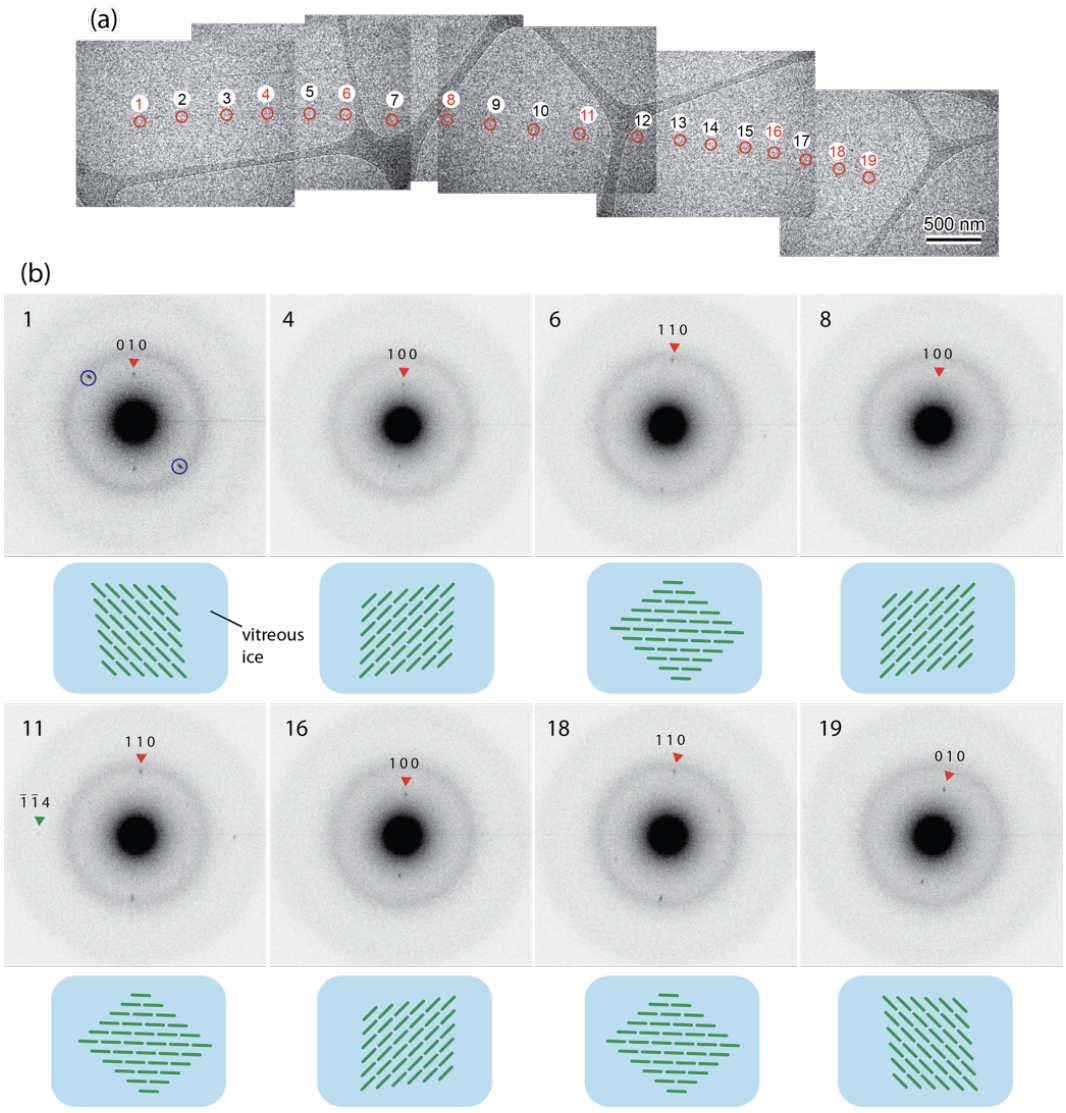

Figure 2. Electron microdiffraction analysis of the twist geometry of *Glaucocystis* CNF in vitreous ice layer. (a) Low-dose diffraction contrast image of studied Glaucocrystis CNF. Circles indicate positions where diffraction patterns were taken. (c) Selected electron diffraction patterns taken from the CNF in (a) together with schematic illustrations of cross-sectional orientation at each position. In these schemes electrons are irradiating from the top side. Circled diffraction spots in the pattern 1 are not from the studied CNF but from another CNF.

A similar electron microdiffraction analysis was carried out with a *Glaucocystis* CNF dried on an amorphous carbon film. The studied CNF was roughly straight without any

visible kinks or defected area. The diffraction patterns were taken with an interval of ca. 300 nm and with an overall length of ca. 6 μm along the single CNF. As in the data set taken under cryo condition (Fig. 2b), the diffraction patterns show different projections of cellulose Iα crystal depending on the acquisition positions, indicative of the presence of fibrillar twist (Fig. 3b). Unlike the continuous twisting of the CNF in the vitreous ice layer, the dry *Glaucocystis* CNF shows a discontinuous twist geometry. The diffraction patterns obtained at the positions from 1 to 7 show the identical projection containing the -1 0 1 reciprocal vector, pointing a presence of a flat segment over about 2 μm. A similar flat segment extends between the positions from 9 to 13. A different projection containing 1 1 0 reciprocal vector is observed at the position 8 which locates between two flat segments. This means that the CNF is twisted sharply by 180° in the length of about 600 nm between the positions 7 and 9. The alternate occurrence of flat segments and a sharp twist region is clearly different from the continuous twisting of the CNF in the vitreous ice. The twist geometry of *Glaucocystis* CNFs is thus altered upon drying on the flat carbon substrate. A similar alteration of the twist geometry upon drying was observed for the tunicate CNCs and likely a common phenomenon for isolated cellulose nanoparticles (Ogawa, 2019).

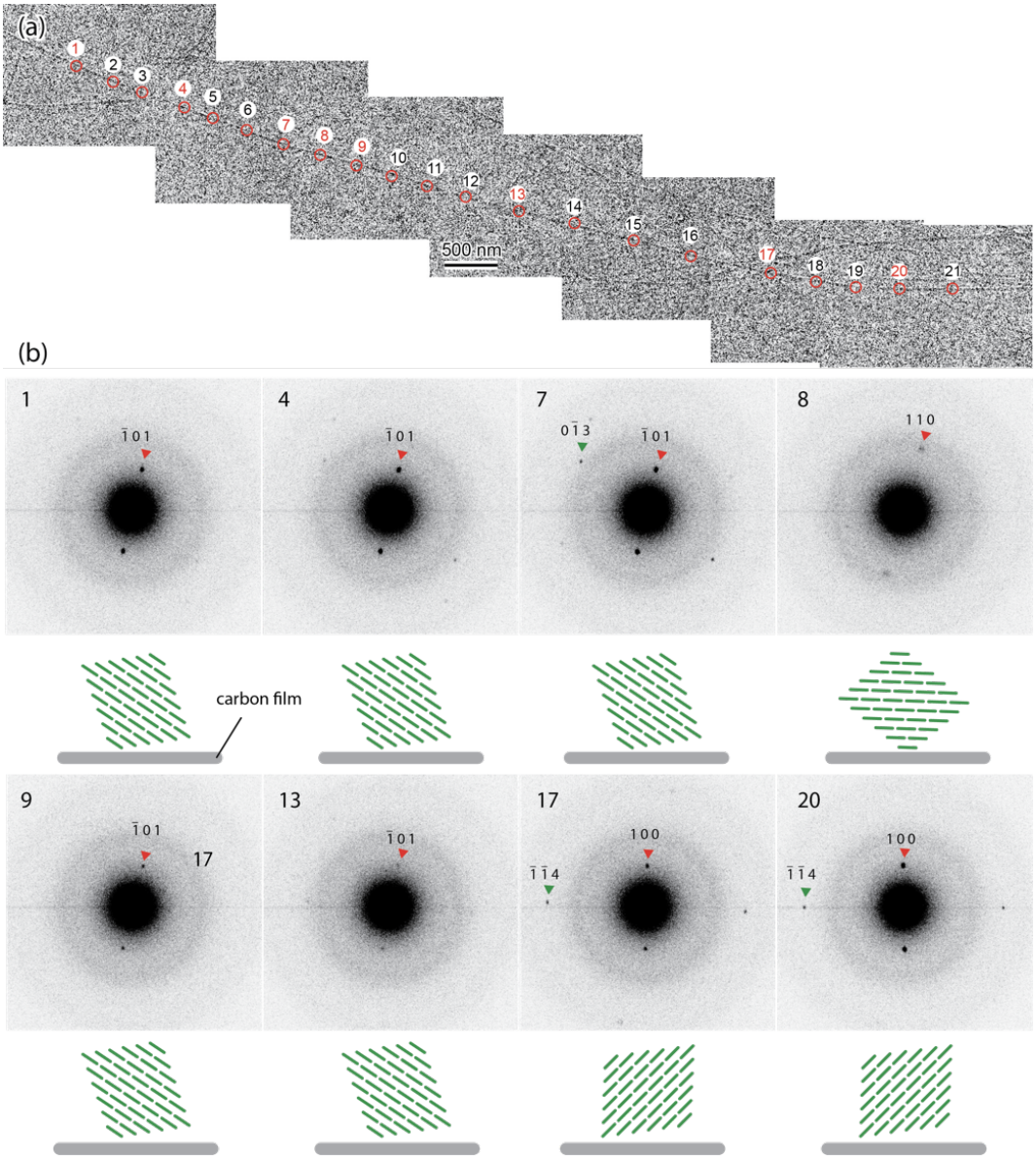

Figure 3. Electron microdiffraction analysis of the twist geometry of *Glaucocystis* CNF dried on an amorphous carbon film. (a) Low-dose diffraction contrast image of studied *Glaucocrystis* CNF. Circles indicate positions where diffraction patterns were taken. (c) Selected electron diffraction patterns taken from the CNF in (a) together with schematic illustrations of cross-sectional orientation at each position. In these schemes electrons are irradiating from the top side.

4. Discussion

The present electron microdiffraction analyses have clearly demonstrated that when extracted from their cell wall the individual *Glaucocystis* CNFs are twisted in both the aqueous and the dry conditions. As abovementioned their twists are less visible compared to those of other cellulose nanoparticles likely due to their square cross sections (Fig. 1). The electron diffraction-based analysis is thus essential to reveal the detailed twist geometry of the *Glaucocystis* CNFs.

Such fibrillar twists are absent in the cellulose microfibrils in the *Glaucocystis* cell wall as aforementioned the introduction. This difference in the fibril morphologies *in vivo* and in the isolated state indicates that the fibrillar twist is introduced during the isolation process, where the occurrence of the twists suggests that the twisting arises as a consequence of relaxation from mechanical constraints pre-existing in the cell wall. Such constraints can originate from various reasons from biosynthesis mechanisms of cellulose microfibrils and their tight packing in the lamellar structure, to surface interactions of the microfibrils with other materials in the cell wall. In the cellulose biosynthesis the cellulose microfibrils are secreted from a membrane-bound protein complex, namely cellulose synthase complex (CSC) (Turner & Kumar, 2018). The CSC moves on the plasma membrane plane as it deposits a microfibril which is anchored on the cell surface (Paredez, Somerville, & Ehrhardt, 2006). This situation imposes a deposition of microfibrils laid flat on the cell surface as previously proposed. The tight packing of microfibrils with matrix materials in the lamella structure would not allow a structural relaxation of the cellulose crystal but further immobilize the flat morphology even when the deposited cellulose layer is detached from the plasma membrane. The removal of the matrix material and the disruption of the cell wall during the microfibril isolation in aqueous environment induce its relaxation with the likely consequence of the twist morphology. While many biological and structural aspects of cellulose biosynthesis are still elusive in both algal and higher plant systems, one should

212 expect a similar geometrical constraint in secretion of cellulose microfibrils in any cellulosic
213 systems. The process-induced twist of the CNFs shown in this study underlines the fact that it
214 is dangerous to assume the occurrence of cellulose twisting *in planta* simply based on
215 observations of twists of isolated nanoparticles.

216 The *Glaucocystis* cellulose studied in this study is composed of almost pure Iα
217 allomorph in contrast to the pure Iβ tunicate cellulose studied in the previous report (Belton,
218 Tanner, Cartier, & Chanzy, 1989). Despite having different allomorphs, the two specimens,
219 *Glaucocystis* CNF and tunicate CNC show similar continuous twist geometries with twisting
220 rates of the same order of magnitude in vitreous ice layers. While the comparison is yet to be
221 systematically made among cellulose crystals with various Iα/Iβ ratios, this comparison
222 between two extreme examples suggest that the allomorphic structure is not a dominant
223 factor that controls the fibrillar twist geometry of native cellulose crystals.

224 In contrast, the fibril width has a significant effect on the twist morphology. Based on
225 the twist rate and the fibril width measured in the current analysis, one can estimate an
226 applied torque to the studied CNF. In classic solid mechanics, a torque, T, applied to a
227 straight bar is given as

228 $$T = GJ\theta/L$$

229 , where G is a shear modulus, J is torsion constant, θ is a twist angle and L is a length of the
230 bar. The torsion constant is a function of cross-sectional shape and one for a square cross
231 section bar is given as

232 $$J_{square} = 0.1406\, a^4$$

233 , where a is the square side length. The shear modulus G_{ab} of the cellulose crystal was
234 estimated as 3.4 GPa based on a force field simulation (Chen, Ogawa, Nishiyama, Ismail,
235 Mazeau, 2016). The fibril width of the CNF in Fig. 2a is ca. 10 nm and a twist rate of 8°/100
236 nm is used as a representative value, which gives a torque T of 6.67 nN·nm. The cross section

of 10 nm×10 nm of an Iα crystal contains 15 (along *a*-axis) ×17 (along *b*-axis) = 255 molecular chains, so the torque per molecular chain is 26 pN·nm. Based on this torque value, a twist pitch, a fibril length for a 180° turn can be estimated for a cellulose crystal with a given cross section. The higher plant cellulose microfibrils are proposed to have a round cross section composed of 18 molecular chains (Jarvis, 2017; Nixon et al., 2016). The torsion constant of a bar with a round cross section is given as

$$J_{round} = \pi d^4/32$$

where *d* is a fibril diameter. The twist pitch is estimated as 137 nm for a cellulose crystal with a round cross section composed of 18 molecular chains with *d* = 2.8 nm. While the dimensions of a hexagonal cross section, another common cross-sectional model, can be considered approximately the same with the round cross section, a rectangular cross section, (3 × 6 chains, a= 2.8 nm, b = 2 nm) gives a different estimation of the twist pitch. A torsion constant of a bar with a rectangular cross section is given as

$$J_{rectangular} = ab^3\left[\frac{16}{3} - 3.36\frac{b}{a}\left(1 - \frac{b^4}{12a^4}\right)\right].$$

Thus, the estimated twist pitch for this fibril with the rectangular cross section is 95 nm. This value is 44% shorter than that of the round cross section, highlighting the importance of the cross-sectional shape on the twist geometry of cellulose crystals. These estimated pitch values agree with the values based on AFM observations of softwood CNFs (90-140 nm) even though the charge effect is not considered in this current estimation (Arcari et al., 2019). This agreement indicates that the molecular torque is intrinsic to the cellulose molecule and constant regardless of biological origin of cellulose crystals. It also implies that the twist geometry of the isolated cellulose crystals is not depending on their biological origins but on their torsion constant determined by their cross-sectional shapes. Since the torque is intrinsic to the molecule and thus pre-exists in untwisted cellulose microfibrils in a constrained cell

wall architecture, a gentle isolation process without strong mechanical homogenization is enough to induce the fibrillar twists to cellulose crystals.

The twist pitch predicted by theoretical methods shows a large diversity depending on the used methods: for a fibril model with the same square cross section composed of 36 molecular chains with a = 3.6 nm, a force field simulation estimates the pitch as 150 nm, while a density-functional based tight-binding calculation predicts it as 380 nm (Dumitrică, 2020; Zhao et al., 2013). The corresponding twist pitch is estimated as 268 nm based on the torque calculated from the current observation. The validity of the theoretical predictions of the twist geometry has to be confirmed with quantitative experimental observations that have recently become more available.

5. Conclusion

A sequential electron microdiffraction method was applied to the *Glaucocystis* CNFs to investigate the effects of the allomorphic structures and the isolation process on the twist geometry of the cellulose crystals. The microdiffraction method was essential for this investigation since the fibrillar twists of *Glaucocystis* CNFs were barely visible due to their square cross-sectional shape, hindering an imaging-based characterization. The series of electron diffraction patterns obtained under cryogenic condition revealed the presence of the continuous twisting of *Glaucocystis* CNF composed of almost pure Iα crystal in vitreous ice layer. In a similar manner with the previously observed tunicate CNCs, this regular twist was altered to discontinuous sharp twists and flat segments upon drying on flat carbon substrates. Since the cellulose microfibrils are untwisted in the *Glaucocystis* cell wall, this twisting is thus a consequence of the nanofiber isolation treatment. Our study sheds light into the discussion on the presence of the fibrillar twists of cellulose crystals *in vivo*. Further

structural investigations are needed to elucidate whether such twists exist in other algal and higher plant cell walls.

The torque applied to the cellulose crystal was calculated based on the current observation, allowing estimating the twist pitch of crystals of different cross-sectional morphologies. The estimated pitch value for a thinner crystal is in good agreement with the experimental observations of softwood CNFs. This indicates a strong dependence of the twist geometry of isolated cellulose crystals on the cross-sectional sizes and shapes.

Acknowledgement

I thank Dr Yoshiharu Nishiyama, Dr Karim Mazeau, Dr Henri Chanzy, and Mr Pierre Sailler for their help during the writing of this article. I acknowledge the NanoBio-ICMG platform (FR 2607) for granting access to the electron microscopy facility and Glyco@Alps (ANR-15-IDEX-02) for financial support.

Reference

Arcari, M., Zuccarella, E., Axelrod, R., Adamcik, J., Sánchez-Ferrer, A., Mezzenga, R., & Nyström, G. (2019). Nanostructural properties and twist periodicity of cellulose nanofibrils with variable charge density. *Biomacromolecules*, *20*(3), 1288-1296.

Bai, L., Kämäräinen, T., Xiang, W., Majoinen, J., Seitsonen, J., Grande, R., Huan, S., Liu, L., Fan, Y., & Rojas, O. J. (2020). Chirality from Cryo-Electron Tomograms of Nanocrystals Obtained by Lateral Disassembly and Surface Etching of Never-Dried Chitin. *ACS Nano*, 14(6) 6921-6930.

Belton, P. S., Tanner, S. F., Cartier, N., & Chanzy, H. (1989). High-resolution solid-state carbon-13 nuclear magnetic resonance spectroscopy of tunicin, an animal cellulose. *Macromolecules*, 22(4), 1615-1617.

Briois, B., Saito, T., Pétrier, C., Putaux, J. L., Nishiyama, Y., Heux, L., & Molina-Boisseau, S. (2013). I α→ I β transition of cellulose under ultrasonic radiation. *Cellulose*, *20*(2), 597-603.

Chen, P., Ogawa, Y., Nishiyama, Y., Ismail, A. E., & Mazeau, K. (2016). Linear, non-linear and plastic bending deformation of cellulose nanocrystals. *Physical Chemistry Chemical Physics, 18*(29), 19880-19887.

Conley, K., Godbout, L., Whitehead, M. T., & van de Ven, T. G. (2016). Origin of the twist of cellulosic materials. *Carbohydrate polymers*, *135*, 285-299.

Dumitrică, T. (2020). Intrinsic twist in Iβ cellulose microfibrils by tight-binding objective boundary calculations. *Carbohydrate Polymers*, *230*, 115624.

Elazzouzi-Hafraoui, S., Nishiyama, Y., Putaux, J. L., Heux, L., Dubreuil, F., & Rochas, C. (2008). The shape and size distribution of crystalline nanoparticles prepared by acid hydrolysis of native cellulose. *Biomacromolecules*, *9*(1), 57-65.

Fang, L., & Catchmark, J. M. (2014). Characterization of water-soluble exopolysaccharides from Gluconacetobacter xylinus and their impacts on bacterial cellulose crystallization and ribbon assembly. *Cellulose*, *21*(6), 3965-3978.

Fernandes, A. N., Thomas, L. H., Altaner, C. M., Callow, P., Forsyth, V. T., Apperley, D. C., Kennedy, C. J., & Jarvis, M. C. (2011). Nanostructure of cellulose microfibrils in spruce wood. *Proceedings of the National Academy of Sciences*, *108*(47), E1195-E1203.

Foster, E. J., Moon, R. J., Agarwal, U. P., Bortner, M. J., Bras, J., Camarero-Espinosa, S., et al. (2018). Current characterization methods for cellulose nanomaterials. *Chemical Society Reviews*, *47*(8), 2609-2679.

Hanley, S. J., Revol, J. F., Godbout, L., & Gray, D. G. (1997). Atomic force microscopy and transmission electron microscopy of cellulose from *Micrasterias denticulata*; evidence for a chiral helical microfibril twist. *Cellulose*, *4*(3), 209.

Helbert, W., Nishiyama, Y., Okano, T., & Sugiyama, J. (1998). Molecular imaging of *Halocynthia papillosa* cellulose. *Journal of Structural Biology*, *124*(1), 42-50.

Hirai, A., Tsuji, M., & Horii, F. (1998). Helical sense of ribbon assemblies and splayed microfibrils of bacterial cellulose. *Sen'i Gakkaishi*, *54*(10), 506-510.

Kim, N. H., Herth, W., Vuong, R., & Chanzy, H. (1996). The cellulose system in the cell wall of *Micrasterias*. *Journal of Structural Biology*, 117(3), 195-203.

Imai, T., Sugiyama, J., Itoh, T., & Horii, F. (1999). Almost pure Iα cellulose in the cell wall of *Glaucocystis*. *Journal of Structural Biology*, *127*(3), 248-257.

Itoh, T., & Brown, R. M. (1984). The assembly of cellulose microfibrils in *Valonia macrophysa* Kütz. *Planta*, *160*(4), 372-381.

Jakob, H. F., Fratzl, P., & Tschegg, S. E. (1994). Size and arrangement of elementary cellulose fibrils in wood cells: a small-angle X-ray scattering study of *Picea abies*. *Journal of Structural Biology*, *113*(1), 13-22.

Jarvis, M. C. (2018). Structure of native cellulose microfibrils, the starting point for nanocellulose manufacture. *Philosophical Transactions of the Royal Society A: Mathematical, Physical and Engineering Sciences, 376*(2112), 20170045.

Kaushik, M., Basu, K., Benoit, C., Cirtiu, C. M., Vali, H., & Moores, A. (2015). Cellulose nanocrystals as chiral inducers: enantioselective catalysis and transmission electron microscopy 3D characterization. *Journal of the American Chemical Society*, *137*(19), 6124-6127.

356 Mao, Y., Liu, K., Zhan, C., Geng, L., Chu, B., & Hsiao, B. S. (2017). Characterization of
357 nanocellulose using small-angle neutron, X-ray, and dynamic light scattering
358 techniques. *The Journal of Physical Chemistry B*, *121*(6), 1340-1351.
359 Majoinen, J., Hassinen, J., Haataja, J. S., Rekola, H. T., Kontturi, E., Kostiainen, M. A., Ras,
360 R. H. A., Törmä, P., & Ikkala, O. (2016). Chiral plasmonics using twisting along
361 cellulose nanocrystals as a template for gold nanoparticles. *Advanced*
362 *Materials*, *28*(26), 5262-5267.
363 Mastronarde, D. N. (2003). SerialEM: a program for automated tilt series acquisition on
364 Tecnai microscopes using prediction of specimen position. *Microscopy and*
365 *Microanalysis*, *9*(S02), 1182-1183.
366 Matthews, J. F., Skopec, C. E., Mason, P. E., Zuccato, P., Torget, R. W., Sugiyama, J.,
367 Himmel, M. E., & Brady, J. W. (2006). Computer simulation studies of
368 microcrystalline cellulose Iβ. *Carbohydrate research*, *341*(1), 138-152.
369 Nakai, T., Sugano, Y., Shoda, M., Sakakibara, H., Oiwa, K., Tuzi, S., Imai, T., Sugiyama, J.,
370 Takeuchi, M., Yamauchi, D., & Mineyuki, Y. (2013). Formation of highly twisted
371 ribbons in a carboxymethylcellulase gene-disrupted strain of a cellulose-producing
372 bacterium. *Journal of Bacteriology*, *195*(5), 958-964.
373 Nishiyama, Y., Sugiyama, J., Chanzy, H., & Langan, P. (2003). Crystal structure and
374 hydrogen bonding system in cellulose Iα from synchrotron X-ray and neutron fiber
375 diffraction. *Journal of the American Chemical Society*, *125*(47), 14300-14306.
376 Nixon, B. T., Mansouri, K., Singh, A., Du, J., Davis, J. K., Lee, J. G., Slabaugh, E.,
377 Vandavasi, V. G., O'Neill, H., Roberts, E. M., Roberts, A. W., Yingling, Y. G., &
378 Haigler, C. H. (2016). Comparative structural and computational analysis supports
379 eighteen cellulose synthases in the plant cellulose synthesis complex. *Scientific*
380 *Reports, 6*(1), 28696.

Ogawa, Y. (2019). Electron microdiffraction reveals the nanoscale twist geometry of cellulose nanocrystals. *Nanoscale*, *11*(45), 21767-21774.

Park, Y. B., Lee, C. M., Koo, B. W., Park, S., Cosgrove, D. J., & Kim, S. H. (2013). Monitoring meso-scale ordering of cellulose in intact plant cell walls using sum frequency generation spectroscopy. *Plant Physiology*, *163*(2), 907-913.

Paredez, A. R., Somerville, C. R., & Ehrhardt, D. W. (2006). Visualization of cellulose synthase demonstrates functional association with microtubules. *Science*, *312*(5779), 1491-1495.

Sugiyama, J., Chanzy, H., & Revol, J. F. (1994). On the polarity of cellulose in the cell wall of *Valonia*. *Planta*, *193*(2), 260-265.

Turner, S., & Kumar, M. (2018). Cellulose synthase complex organization and cellulose microfibril structure. *Philosophical Transactions of the Royal Society A: Mathematical, Physical and Engineering Sciences*, *376*(2112), 20170048.

Usov, I., Nyström, G., Adamcik, J., Handschin, S., Schütz, C., Fall, A., Bergström, L., & Mezzenga, R. (2015). Understanding nanocellulose chirality and structure–properties relationship at the single fibril level. *Nature Communications*, *6*(1), 1-11.

Willison, J. H., & Brown Jr, R. M. (1978). Cell wall structure and deposition in *Glaucocystis*. *The Journal of Cell Biology*, *77*(1), 103-119.

Zhao, Z., Shklyaev, O. E., Nili, A., Mohamed, M. N. A., Kubicki, J. D., Crespi, V. H., & Zhong, L. (2013). Cellulose microfibril twist, mechanics, and implication for cellulose biosynthesis. *The Journal of Physical Chemistry A*, *117*(12), 2580-2589.